Monthly Notices of the ROYAL ASTRONOMICAL SOCIETY

MNRAS **468,** 2684–2698 (2017) doi:10.1093/mnras/stx616
Advance Access publication 2017 March 24

Low-mass young stellar population and star formation history of the cluster IC 1805 in the W4 H II region

Neelam Panwar,[1,2]★ M. R. Samal,[2,3]★ A. K. Pandey,[4] J. Jose,[5] W. P. Chen,[2] D. K. Ojha,[6] K. Ogura,[7] H. P. Singh[1] and R. K. Yadav[8]

[1]*Department of Physics and Astrophysics, University of Delhi, Delhi 110007, India*
[2]*Graduate Institute of Astronomy, National Central University 300, Jhongli City, Taoyuan County 32001, Taiwan*
[3]*Laboratoire d'Astrophysique de Marseille-LAM, Université d'Aix-Marseille and CNRS, UMR7326 F-13388 Marseille CEDEX 13, France*
[4]*Aryabhatta Research Institute of Observational Sciences (ARIES), Nainital 263129, India*
[5]*Kavli Institute for Astronomy and Astrophysics, Peking University, 5 Yiheyuan Road, Haidian District, Beijing 100871, People's Republic of China*
[6]*Tata Institute of Fundamental Research, Mumbai 400 005, India*
[7]*Kokugakuin University, Higashi, Shibuya-ku, Tokyo 1508440, Japan*
[8]*National Astronomical Research Institute of Thailand (NARIT), Chiang Mai 50200, Thailand*

Accepted 2017 March 10. Received 2017 March 10; in original form 2016 February 5

ABSTRACT

W4 is a giant H II region ionized by the OB stars of the cluster IC 1805. The H II region/cluster complex has been a subject of numerous investigations as it is an excellent laboratory for studying the feedback effect of massive stars on the surrounding region. However, the low-mass stellar content of the cluster IC 1805 remains poorly studied till now. With the aim to unravel the low-mass stellar population of the cluster, we present the results of a multiwavelength study based on deep optical data obtained with the Canada–France–Hawaii Telescope, infrared data from Two Micron All Sky Survey and *Spitzer Space Telescope* and X-ray data from *Chandra Space Telescope*. The present optical data set is complete enough to detect stars down to 0.2 $M_{\odot}$, which is the deepest optical observation so far for the cluster. We identified 384 candidate young stellar objects (YSOs; 101 Class I/II and 283 Class III) within the cluster using various colour–colour and colour–magnitude diagrams. We inferred the mean age of the identified YSOs to be ∼2.5 Myr and mass in the range 0.3–2.5 $M_{\odot}$. The mass function of our YSO sample has a power-law index of -1.23 ± 0.23, close to the Salpeter value (-1.35), and consistent with those of other star-forming complexes. We explored the disc evolution of the cluster members and found that the disc-less sources are relatively older compared to the disc bearing YSO candidates. We examined the effect of high-mass stars on the circumstellar discs and within uncertainties, the influence of massive stars on the disc fraction seems to be insignificant. We also studied the spatial correlation of the YSOs with the distribution of gas and dust of the complex to conclude that IC 1805 would have formed in a large filamentary cloud.

Key words: stars: formation – stars: pre-main-sequence – HII regions – open clusters and associations: individual: IC 1805.

1 INTRODUCTION

Most recent studies show that stars are formed in clusters or groups and nearly half of the low-mass populations are born in massive young clusters or OB associations (Lada & Lada 2003; Allen et al. 2007). Young clusters are natural laboratories for testing the star formation processes and the stellar evolutionary theory, as the cluster members have a wide mass spectrum while sharing the same chemical composition and distance.

However, the presence of very luminous (O- or early B-type) stars in such systems profoundly influences their environment by compressing and sweeping the surrounding material because of their strong ionizing radiation and powerful stellar winds (see e.g. Preibisch et al. 2002; Zavagno et al. 2007; Chauhan et al. 2009, 2011; Povich et al. 2009; Deharveng et al. 2010; Jose et al. 2013; Samal et al. 2014). Ultraviolet (UV) radiation from massive stars not only affects the surrounding molecular cloud and its star formation but also causes photoevaporation of discs around

★ E-mail: neelam_1110@yahoo.co.in (NP); manash.samal3@gmail.com (MRS)

the young low-mass stars in their vicinity (see e.g. Bally et al. 1998; Adams et al. 2004; Balog et al. 2007; Gorti & Hollenbach 2009), thereby playing a key role in shaping the fundamental properties of the cluster such as stellar mass function (MF), total star formation efficiency and evolution of circumstellar discs around the young stars.

IC 1805, also known as Melotte 15 or OCL 352, is a young open cluster associated with the H II region W4 (the Heart Nebula), which is a part of the W3-W4-W5 complex and contains dozens of massive OB-type stars (Massey, Johnson & Degioia-Eastwood 1995). The W4 complex evacuated by the combined energetic winds of the OB stars within IC 1805 (Goudis & White 1980; Ninkov et al. 1995) appears to be a void in the atomic hydrogen layer with a width of about 100 pc (Taylor et al. 1999). The W4 complex also contains several cometary-shaped bright-rimmed clouds (BRCs) or pillars, pointing towards the luminous stars of IC 1805 (Sugitani, Fukui & Ogura 1991; Lefloch, Lazareff & Castets 1997), similar to those found in Ogura, Sugitani & Pickles (2002) and Chauhan et al. (2011). Such structures are generally the result of compression and erosion of pre-existing clouds by massive stars (Bisbas et al. 2009; Miao et al. 2009), indicating that stellar feedback is playing a strong role in altering the morphology and physical conditions of the W4 complex. Therefore, the complex has been a subject of numerous investigations for understanding the role of massive stars on the star formation process in the surrounding cloud (e.g. Lada et al. 1978; Taylor et al. 1999; Oey et al. 2005; Koenig et al. 2012; Jose et al. 2016).

IC 1805 is located at a moderate distance of ∼2.0 kpc (Straižys et al. 2013), similar to the adjacent H II regions W3 (2.0 kpc; Hachisuka et al. 2006; Xu et al. 2006) and W5 E (2.1 kpc; Chauhan et al. 2011). It is embedded in a very low extinction cloud of $E(B-V) \sim 0.8$ mag or visual extinction (A_v) ∼ 2.4 mag (Joshi & Sagar 1983; Straižys et al. 2013). Also, according to Guetter & Vrba (1989), Sagar & Yu (1990) and Hanson & Clayton (1993), the extinction law in the direction of IC 1805 is normal. Hence, it is a good target for studies on star formation and evolution of low-mass stars; in particular, how they are influenced by OB-type stars. Though the cluster has been investigated by several authors at optical bands (Joshi & Sagar 1983; Kwon & Lee 1983; Sagar 1987; Guetter & Vrba 1989; Massey et al. 1995; Ninkov et al. 1995; Sung & Lee 1995), most of these studies were limited to the high-mass stars only. These observations were not only too shallow to detect the low-mass stellar populations but also cover only a relatively small area of the complex. Similarly, although several attempts have been made to identify young stellar objects (YSOs) in the complex (Koenig et al. 2012; Broos et al. 2013; Povich et al. 2013; Straižys et al. 2013), no adequate attention has been paid to the characterization of low-mass young stellar population of the cluster using deep optical photometric data.

Since low-mass stars constitute the majority of the stellar population in a cluster and even in the Galaxy (Kroupa 2002), the low-mass stellar content and its MF are essential to understand the nature of the star formation process and the properties of open clusters. Young stars can be identified using multiwavelength observations depending on their evolutionary stages and spectral types (e.g. Carpenter et al. 2006; Dahm & Hillenbrand 2007). Overall, the *Spitzer* results suggest that though primordial circumstellar discs around solar and sub-solar mass stars can last for up to 10 Myr, disc lifetimes are a factor of 2 shorter for higher mass objects (see Williams & Cieza 2011, and references therein).

The infrared (IR) observations are particularly useful to identify pre-main-sequence (PMS) stars exhibiting IR excess emission.

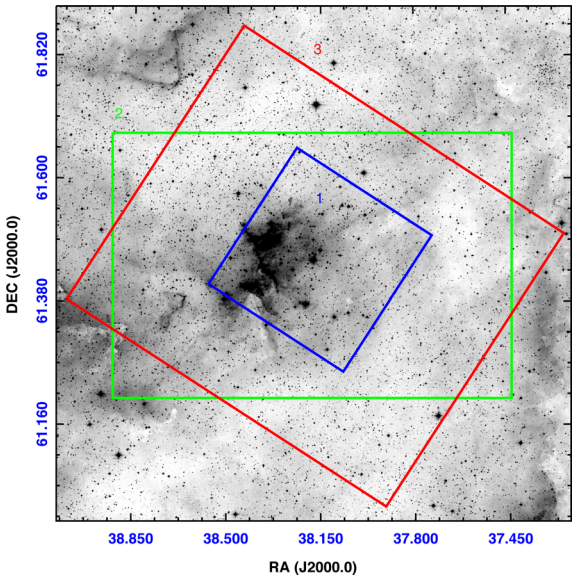

Figure 1. The DSS2-R image of the IC 1805 H II region. The area covered by X-ray, optical and *Spitzer*–IRAC observations are shown with blue, green and red colours, respectively (also marked as '1', '2' and '3').

Also, with the help of X-ray data, young stars can be identified from their excess X-ray emission due to magnetic reconnection flares similar to those seen on the solar surface, but with X-ray fluxes two to three orders of magnitude larger in comparison to solar-type stars (Feigelson & Montmerle 1999; Preibisch & Feigelson 2005; Güdel et al. 2007). While near-infrared (NIR), mid-infrared (MIR) and X-ray observations are suitable to identify PMS stars, they have limitations in characterization of these stars themselves (e.g. age and mass determinations). This can be done best by optical observations as PMS stars possess little or no circumstellar emission at optical wavelengths.

In this work, we attempt to investigate the low-mass stellar content of the cluster IC 1805 based on high spatial resolution, deep optical photometric observations taken with the Canada–France–Hawaii Telescope (CFHT) in combination with *Spitzer*, Two Micron All Sky Survey (2MASS) and X-ray data available for the region. We identify and characterize a sample of low-mass young cluster members with circumstellar discs and evolved disc-less candidate members. We examine the physical properties of the cluster (e.g. cluster extent, age, disc evolution and MF) and try to understand the star formation process in this region.

2 OBSERVATIONS AND DATA REDUCTION

Fig. 1 shows the DSS2-R image of the IC 1805 region. The regions marked in blue, green and red are the areas covered by X-ray, optical and *Spitzer*–Infrared Array Camera (IRAC) observations, respectively. Multiband Imaging photometer for Spitzer (MIPS) observations are available for the entire area covered by the IRAC observations. The individual observations and photometric catalogues are described below.

2.1 Optical observations

The pre-processed deep *V*- and *R*-band images of the IC 1805 region were obtained from the CFHT archive. The data were obtained with CFH12K, a mosaic CCD camera on CFHT, on 2002 January

Table 1. The zero-point constants, colour coefficients and extinction coefficients.

Parameters	Constants
Zero-point constants	
c1	-0.226 ± 0.016
c2	3.114 ± 0.014
Colour coefficients	
m1	1.058 ± 0.022
m2	0.099 ± 0.024
Extinction coefficients	
K_v	0.158 ± 0.015
K_r	0.109 ± 0.011

07 (P. I. – Sung H.). With a plate scale of 0.21 arcsec per pixel, CFH12K provides a 42 arcmin × 28 arcmin field of view (FOV). Three exposures of 150 s were taken in the *V* and *R* bands each and the typical seeing during the observations was ∼0.9 arcsec. We obtained the photometry of the stars by using the standard IRAF tasks and DAOPHOT-II software package (Stetson 1987). We used the DAOFIND task in IRAF to extract the point sources and selected only those sources having S/N 5σ above the background. We then performed point-spread function (PSF) photometry on the selected sources using the ALLSTAR routine. These deep optical observations were obtained from the archive with the aim to characterize the low-mass members (in particular, to obtain the age and mass of the low-mass young stellar population) of the cluster IC 1805. To calibrate these deep images, we obtained the *V*- and *R*-band observations of the central region of IC 1805 on 2012 October 26 by using a 2048 × 2048 pixel^2 CCD camera mounted at the f/4 Cassegrain focus of the 1.3-m Devasthal Optical Telescope (DOT) at Aryabhatta Research Institute of Observational Sciences, Nainital, India. The CCD camera with a pixel size 13.5 μm and a plate scale 0.54 arcsec per pixel, covers an ∼18 arcmin × 18 arcmin FOV. During the observations the seeing was ∼1.5 arcsec. To standardize the observations, the SA 98 field of Landolt (1992) was also observed on the same night at various airmasses. A number of bias and twilight flat frames were also taken during the observations.

The DOT images were reduced using various tasks available in the IRAF software package. Instrumental magnitudes were obtained by using the IRAF/DAOPHOT-II package via PSF fitting. The PSF was obtained for each frame by using several isolated stars in the frames. The atmospheric extinction coefficients and zero-point magnitudes obtained from the SA 98 standard field observations are given in Table 1. The instrumental magnitudes were converted to the standard values by using a least-squares linear regression procedure outlined by Stetson (1992). The following transformation equations were used to calibrate the observations:

$$(V - R) = m_1(v - r) + c_1,$$

$$V = v + m_2(v - r) + c_2,$$

where *v, r* are the instrumental magnitudes corrected for the atmospheric extinctions, and *V, R* are the standard magnitudes; c_1, c_2 and m_1, m_2 are zero-point constants and colour coefficients, respectively. The final photometry from the DOT observations is used to calibrate the CFHT photometry. We obtained 27 427 sources with a magnitude uncertainty ≤0.2 mag in both the *v* and *R* bands.

2.2 *Spitzer*–IRAC observations

The NIR/MIR data from the *Spitzer space telescope* (Werner et al. 2004) using IRAC (Fazio et al. 2004) centred at 3.6, 4.5, 5.8 and 8.0 μm were obtained from the *Spitzer* archive.[1] The IRAC camera provides simultaneous 5.2 arcmin × 5.2 arcmin images in four bands at 3.6, 4.5, 5.8 and 8.0 μm and at a spatial resolution of ∼2 arcsec. IC 1805 was observed in 2006 September (P.I. – S. Wolff, Program ID – 20052). The corrected Basic Calibrated Data (cBCD) images of the region (Spitzer Science Center's IRAC pipeline, version S18.14.0) were obtained by using the LEOPARD software. The images were taken in the high dynamical range mode. Both short (0.6 s) and long (12 s) integration cBCD frames in each channel were separately mosaicked using MOPEX (version 18.3.1). The MOPEX-APEX pipeline was used to detect the point sources and to perform the point response function (PRF) fitting photometry. Since the nebular emissions can mimic point-like sources, especially in 5.8 and 8.0 μm, all the sources were visually examined and ambiguous sources were removed. In addition, we also included point sources manually that were not automatically detected by APEX and supplied the list of these sources to *Apex-user-list* pipeline to perform the PRF photometry. We have adopted the zero-points for the conversion between flux densities and magnitudes to be 280.9, 179.7, 115.0 and 64.1 Jy in the 3.6, 4.5, 5.8 and 8.0 μm bands, respectively, as given in Reach et al. (2005). The sources with photometric uncertainties ≤0.2 mag in each band were considered as good detection. To obtain the final catalogue of the sources detected in all IRAC bands, we made a catalogue for each channel from the short and long exposures separately and then looked for the closest match within 1.2 arcsec. The final catalogue contains 32 014 sources that are detected at least in two IRAC bands, of which 5288 sources have photometry in all IRAC bands.

2.3 *Spitzer* MIPS observations

The region was observed at MIPS 24 μm in 2005 September (P.I. – J. S. Greaves, Program ID – 3234). We downloaded the MIPS post-BCD images from the archive, which were created at the image scale of 2.45 arcsec per pixel and at a spatial resolution of ∼6 arcsec. We supplied a list of coordinates of visually identified sources to the *Apex-user-list* module and performed the PRF fitting to extract the fluxes of the sources. The zero-point value 7.14 Jy (adopted from MIPS Data Handbook[2]) is used to convert the flux densities to magnitudes. We cross-matched the MIPS catalogue to the IRAC source catalogue using a matching radius of 2.5 arcsec (Megeath et al. 2012; Jose et al. 2016) and found that 164 sources have counterparts in one or more IRAC bands.

2.4 NIR photometry from 2MASS

NIR JHK_s data for the point sources within the H II region (shown in Fig. 1) have been obtained from the 2MASS Point Source Catalog (Cutri et al. 2003). Sources with uncertainty ≤0.2 mag and quality flag 'AAA' in all the three bands were selected to ensure good quality data. The spatial resolution of 2MASS JHK_s bands is ∼2 arcsec.

[1] http://archive.spitzer.caltech.edu/

[2] http://irsa.ipac.caltech.edu/data/SPITZER/docs/mips/mipsinstrumenthandbook/

3 RESULTS

3.1 Identification and classification of YSOs

Complete understanding of cluster properties and its star formation history requires proper identification of cluster members. In the absence of spectroscopic observations, one robust approach is to identify the young stellar content using multiwavelength photometric observations. Since IC 1805 is located at a low Galactic latitude, the contamination from background/foreground stars may significantly affect the analyses at IR bands (e.g. Getman et al. 2006; Roccatagliata et al. 2011). Hence, careful identification and classification of probable YSO members is essential. During their early phase, stars possess circumstellar discs and hence show excess emission at IR wavelengths. The IR excess properties of YSOs can be used to identify and classify them. Class '0' sources emit most of their radiation in far-infrared (FIR) to submillimetre regime of the electromagnetic spectrum (André 1995). In the Class 'I' phase, YSOs radiate mostly in MIR-FIR wavelengths, whereas Class 'II' sources exhibit NIR-FIR excess emission. Class 'III' sources possess little or no excess in IR (Adams, Lada & Shu 1987; Lada 1987; André, Ward-Thompson & Barsony 1993; André 1995) but show enhanced X-ray activities as explained in Section 3.1.4. However, sources that lack inner discs and show excess emission in MIR wavelengths are referred to as 'transition disc' sources (Hernández et al. 2006; Muzerolle et al. 2006). We used optical, *Spitzer*-IRAC-MIPS, 2MASS and X-ray data sets to identify and classify the YSOs in IC 1805. The various selection criteria adopted for identification and classification of those YSOs are given below.

3.1.1 *YSOs selected by IRAC colours*

Since YSOs occupy distinct positions on the IRAC colour–colour diagrams due to their different characteristics, the colour–colour diagrams are widely used to identify and classify YSO population in a star-forming region (Allen et al. 2004; Megeath et al. 2004). Gutermuth et al. (2009) developed a method consisting of a series of IRAC/MIPS colour criteria to identify and classify YSOs. Though the MIR and FIR observations can penetrate deep into the thick layers of dust and gas and reveal the embedded YSO population, they also enhance the chances of inclusion of background contaminants in the YSO sample. For example, polycyclic aromatic hydrocarbon (PAH)-emitting galaxies, active galactic nuclei (AGNs), unresolved blobs of shocked emission etc. may mimic YSOs and, thus, can contaminate our YSO sample. In order to weed out possible contaminants, we used the customized cuts in the [4.5] − [5.8] versus [5.8] − [8.0] and [3.6] − [5.8] versus [4.5] − [8.0] colour–colour spaces, as described by Gutermuth et al. (2009). After excluding the contaminants based on the Gutermuth et al. (2009) approach, we identified 238 YSO candidates. Of these, four sources satisfy the colour criteria of Class I sources ([4.5]–[5.8] > 0.7 and [3.6]–[4.5] > 0.7) and 234 sources (satisfying the following conditions) were classified as Class II candidates:

$$[4.5] - [8.0] - \sigma > 0.5,$$

$$[3.6] - [5.8] - \sigma > 0.35,$$

$$[3.6] - [5.8] + \sigma \leq (0.14/0.04) \times (([4.5] - [8.0] - \sigma) - 0.5) + 0.5 \text{ and}$$

$$[3.6] - [4.5] - \sigma > 0.15.$$

Here, σ is the photometric uncertainty in respective colours. The rest of the sources may be Class III or field stars. However, it is to be noted that in a few cases, due to reddening and disc inclination effects, a Class II source could mimic the colours of a Class I source (Whitney et al. 2003; Gutermuth et al. 2009). Fig. 2(a) shows the [3.6] − [4.5] versus [5.8]–[8.0] colour–colour diagram for all the uncontaminated IRAC sources. The Class I and Class II sources are shown as red squares and blue diamonds, respectively.

3.1.2 *YSOs from 2MASS/IRAC*

At the central region of W4, in the vicinity of IC 1805, the background emission at 5.8 and 8.0 μm is high compared to the emission at 3.6 and 4.5 μm. This high background emission is often observed in massive star-forming regions (e.g. Indebetouw et al. 2007; Koenig et al. 2008; Ojha et al. 2011). Many of the sources detected in 3.6 and 4.5 μm may be missing in 5.8 and 8.0 μm bands due to the enhanced nebulosity of the background. To ascertain the nature of these sources, we combined the IRAC 3.6 and 4.5 μm data with those of 2MASS H and K_s bands. Gutermuth et al. (2009) used the intrinsic (K_s − [3.6]) versus ([3.6] − [4.5]) colour criteria to identify the sources that are detected at 3.6 and 4.5 μm and possess counterparts in 2MASS bands.

To identify the YSOs using IRAC and 2MASS data, we first created an extinction map based on 2MASS data following the method discussed in Panwar et al. (2014), and then derived the intrinsic colours of the YSOs by correcting for the extinction values read off from this map. To generate the extinction map, we divided the region into small cells and computed the colour excess in each cell using the relation $E = (H - K_s)_{\rm obs} - (H - K_s)_{\rm int}$, where $(H - K_s)_{\rm obs}$ is the observed median colour of the stars in a cell and $(H - K_s)_{\rm int}$ is the intrinsic median colour of the control field stars. The colour excess ratios presented in Flaherty et al. (2007) have been adopted to calculate the extinction in the K_s band (A_{K_s}) for each cell by using the relation A_{K_s}=1.82 E. Based on the extinction map, the mean A_{K_s} in the cluster direction corresponds to $A_v \sim 2.6$ mag, which is comparable to the value reported in the literature (Joshi & Sagar 1983). We calculated the $(K_s - [3.6])_0$ and $([3.6] - [4.5])_0$ colours of the sources and used various colour cuts as described in Gutermuth et al. (2009) to select Class I and Class II sources. By this method, we obtained 161 Class II and six Class I candidates. Among these, based on the IRAC colours, five Class I sources have been classified as Class II (Section 3.1.1), and for further analyses we have considered them as Class II candidates. Out of these 167 Class I/II candidates, 133 were identified by using IRAC colour–colour diagram. Fig. 2(b) shows the 2MASS/IRAC colour–colour diagram for sources having K_s, 3.6 and 4.5 μm detection.

3.1.3 *YSOs from MIPS 24 μm*

To identify the transition disc candidates, we used the 24 μm data in addition to 4.5 and 5.8 μm data. Following Muzerolle et al. (2006) and Hernández et al. (2006), sources mainly with photospheric radiation in the IRAC or IRAC/2MASS classification but having excess emission at 24 μm ([5.8] − [24] > 2.5 and/or [4.5] − [24] > 2.5) are reconsidered as transition disc sources. We identified eight such sources. Since heavily embedded Class II sources can be misclassified as Class I based on the IRAC colour criteria (see Section 3.1.1), those Class I sources with 24 μm data were rechecked to ensure that their SEDs rise from the IRAC to MIPS bands. All Class I candidates were considered as Class II, if they do not have [5.8] − [24] > 4

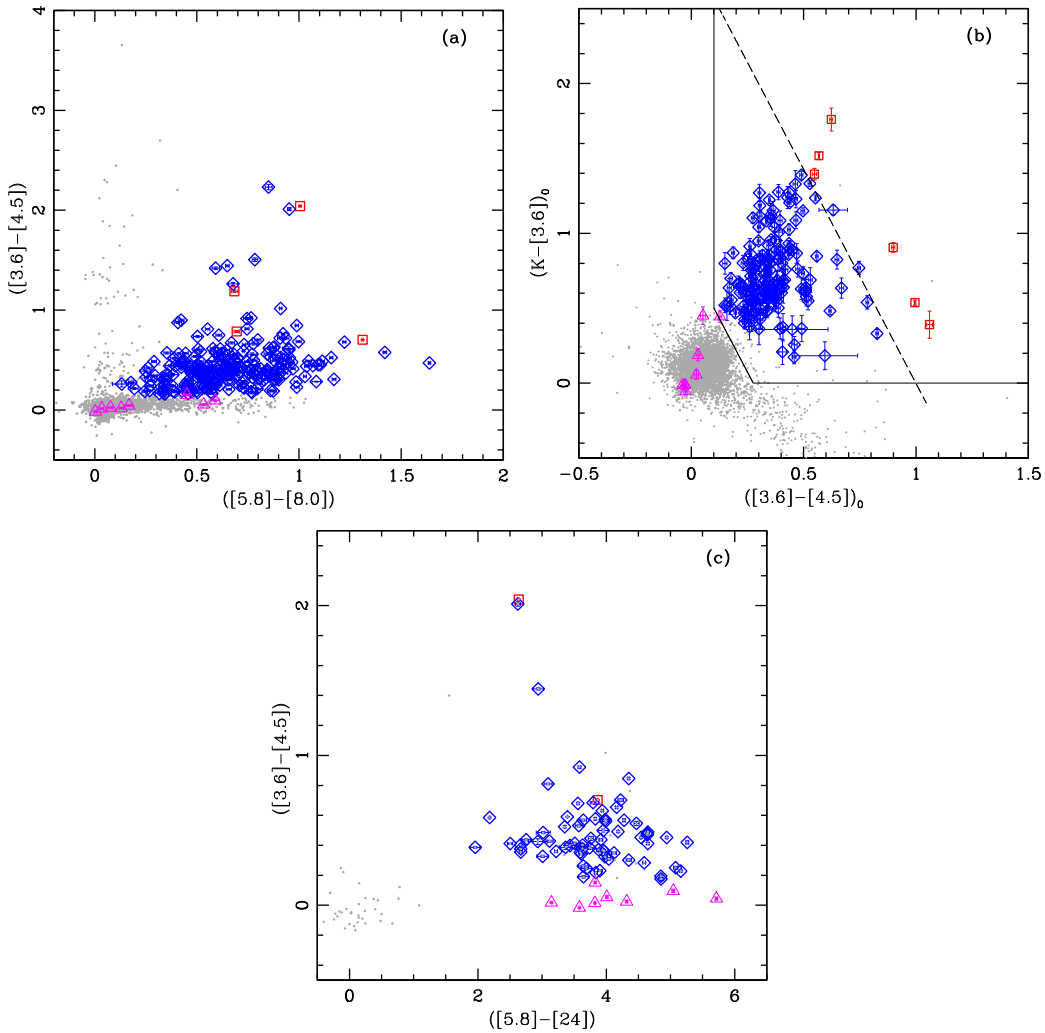

Figure 2. (a) IRAC ([3.6]–[4.5])/([5.8]–[8.0], (b) IRAC/2MASS and (c) IRAC/MIPS colour–colour diagrams for the sources (black dots) in IC 1805. The error bars represent the 1σ uncertainty in respective colours. Class I and Class II sources are shown with red square and blue diamond symbols, respectively. Transition disc candidates are shown with magenta triangles.

or [4.5] − [24] > 4. Out of four Class I sources identified in Section 3.1.1, two are reclassified as Class II, while the remaining two do not possess 24 μm measurements. Fig. 2(c) shows the IRAC/MIPS colour–colour diagram for the sources in the region. In Fig. 2, transition disc candidates based on the MIPS photometry are marked as magenta triangles.

3.1.4 YSOs from Chandra X-ray data

YSOs are often strong X-ray emitters compared to their main-sequence (MS) counterparts (e.g. Feigelson & Montmerle 1999; Getman et al. 2005; Preibisch & Feigelson 2005; Güdel et al. 2007). Hence, X-ray surveys of star-forming regions are used to uncover YSO populations. For the detection of disc-less YSOs, that is, Class III sources, X-ray observations complement the IR YSO sample to have a more complete census of the stellar content of clusters (e.g. Preibisch & Feigelson 2005; Pandey et al. 2013a, 2014). The Massive Star-Forming Regions Omnibus X-ray Catalog (Townsley et al. 2014) detected X-ray sources in a sample of massive star-forming regions, including IC 1805. They characterized the X-ray properties of 647 stars in the IC 1805 using *Chandra*/ACIS observations. ACIS-I consists of four 1024 × 1024 pixel^2 CCD chips that cover a 17 arcmin × 17 arcmin FOV, and covers the 0.5–8.0 keV energy band with a spectral resolution of ∼150 eV at 6 keV and a PSF radius of 0.5 arcsec within ∼2 arcmin of the on-axis position, degrading to ∼6 arcsec at a 10 arcmin off-axis angle. We checked these *Chandra* X-ray sources for the counterparts of our optical data set with a less stringent matching radius of 3 arcsec (Pandey et al. 2013a) because of the large off-axis beam. The agreement between X-ray and optical positions is excellent in majority of the cases (∼80 per cent), with offsets <1 arcsec. In a few cases, where there was more than one source within the matching radius, we considered the closest one as the best match. This search revealed possible optical counterparts to 403 (62 per cent) of the X-ray sources.

Fig. 3 shows V versus $(V - R)$ colour–magnitude diagram (CMD) for the stars in the area covered by X-ray observations. The MS from Girardi et al. (2002) for the solar metallicity is also plotted. Joshi & Sagar (1983) have found that in the direction of IC 1805, $E(B - V) = 0.7$–0.9 mag, indicating a small variation of extinction within the cluster in agreement with the $A_v = 2.2$–2.7 mag,

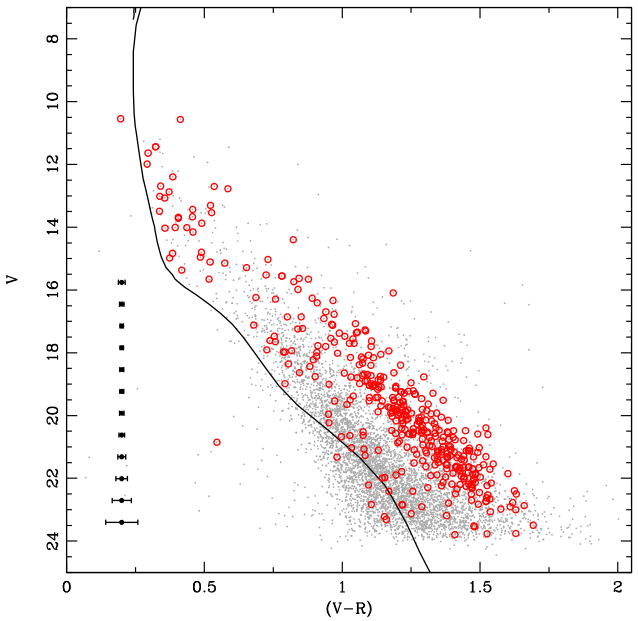

Figure 3. $V/(V-R)$ CMD for the stars in the region covered by X-ray observations (grey dots). The MS from Girardi et al. (2002), corrected for the adopted distance and reddening are also overplotted. The average error in $(V-R)$ colour as a function of magnitude is shown in the left-hand side. Red circles represent the X-ray sources in the region.

estimated by Straižys et al. (2013) from the 39 members of the cluster. The MS is shifted for the adopted distance of 2.0 kpc and the minimum reddening $E(B-V)$ of 0.7 mag. Our approach of using the minimum reddening is consistent with the studies of open clusters (e.g. Sung & Bessell 2004; Sharma et al. 2006; Pandey et al. 2013a). The optical counterparts of the X-ray sources are shown with red circles. In Fig. 3, at the low-luminosity end, one can notice a few X-ray sources scattered close to MS. A similar distribution of X-ray sources close to MS has also been observed in the CMD of other young clusters. For example, the distribution of X-ray sources on the V versus $(V-I)$ diagram of NGC 6530 (median age ∼2.3 Myr and mean $E(B-V) = 0.35$; Prisinzano et al. 2005) shows that 90 per cent of PMS stars are within 0.3–10 Myr and ∼10 per cent of the X-ray sources are outside this age range. Prisinzano et al. (2005) argued that the latter sources are mainly contaminants.

Marino, Micela & Peres (2000) have discussed that the coronal activity of X-ray active field stars such as foreground dwarf M star (dMe) and background giants could lead to misidentification as young stars. For example, in Fig. 3, a few X-ray emitting sources are falling to the left or close to MS. Based on spectroscopic observations of the MS stars, Massey et al. (1995) have inferred that the cluster is likely to be younger than 5 Myr. Considering the young age of the cluster, these sources are unlikely to be part of the cluster. Similarly, extended extragalactic objects seen along the line of sight could also be misidentified as young stars (Getman et al. 2006). Since we have performed PSF photometry on our optical images, we expect that the contamination due to extended objects is minimal in our sample; however, we cannot rule out the possible presence of a few point-like extragalactic objects such as quasars. The field star contamination in our sample is quantified in Section 3.1.5, but at least quantitatively, it appears to be consistent with the amount of foreground X-ray contamination expected in the direction of IC 1805.

To remove the X-ray active field stars from our X-ray YSO sample, we considered only those X-ray sources that are located in the empirical YSO zone on the V versus $(V-R)$ CMD (e.g. Allen et al. 2012). To determine the YSO zone, we used the following process iteratively. We arranged the X-ray sources in 0.75 mag bins between $V = 15.0$ and 24 mag. The median and standard deviation (σ) of the $(V-R)$ colour of the YSOs in each bin were calculated and the YSOs having colours greater than 3σ from the median were considered as outliers. The lower and upper limits of the YSO zone in each bin are then taken to be 1.25σ and 2σ around the median colour of the bin. These upper and lower limits are then fitted with polynomials, and the YSOs lying within these upper and lower bounds are taken to be probable members. As discussed in Allen et al. (2012), the lower limits of the magnitude bins are taken closer to the median value because the density of sources quickly increases in the direction perpendicular to the isochrone towards the MS. In particular, foreground dwarfs and background giants may disguise as YSOs by appearing more luminous for a given colour. We note that although the above statistical approach is likely to remove non-YSO X-ray sources, some actual YSOs may also be eliminated. For example, a few X-ray sources located near the MS (where majority of the field stars are populated) could be YSOs, although their chances of being so are low. Spectroscopic observations are needed to ascertain the nature of such sources, because some of them could be YSOs with disc systems seen edge-on that appear underluminous for their colours because of scattering (Sicilia-Aguilar et al. 2005) or members that are significantly older than the mean cluster age.

Using the above approach, we obtained 337 X-ray emitting YSO candidates in the region covered by *Chandra* X-ray observations (for details; see Section 3.2.2). Of these, 40 sources have shown the characteristics of Class I/II candidate YSOs on the basis of 2MASS and *Spitzer* colours (discussed in Sections 3.1.1, 3.1.2 and 3.1.3), so the rest 297 X-ray sources are considered as Class III candidates.

3.1.5 Data completeness and contamination

As in the c2d legacy project (Evans et al. 2003), the peak of the observed luminosity function can be assumed to estimate ≥90 per cent completeness limit (see also Jose et al. 2016). We constructed the luminosity functions for each band by using the histogram method (see Fig. 4). The resultant completeness limits of the optical and IRAC data are given in Table 2.

For cross-checking, the completeness limits of the V and R bands were also estimated by the artificial star experiment by using ADDSTAR routine in IRAF (e.g. Jose et al. 2013; Pandey et al. 2013b). We randomly added artificial stars of various magnitudes into each image. The luminosity distribution of artificial stars was chosen in such a way that more stars were inserted towards the fainter magnitude bins. The frames were then re-reduced by using the same procedure as used for the original frames (see Section 2.1). The ratio of the number of stars recovered to those added in each magnitude interval gives the completeness factor as a function of magnitude. We thus obtained >90 per cent completeness of the photometry to be 22.5 and 22 mag in the V and R bands, respectively, which agrees with that of the histogram analysis.

The estimation of the completeness census of the YSO sample obtained by various colour combinations is rather difficult as it is limited by several factors. For example, bright extended nebulosity in the IRAC bands significantly limits the point source detection. The YSO identification from the 2MASS/IRAC colours is limited by the sensitivity of the 2MASS survey, while that from the IRAC/MIPS

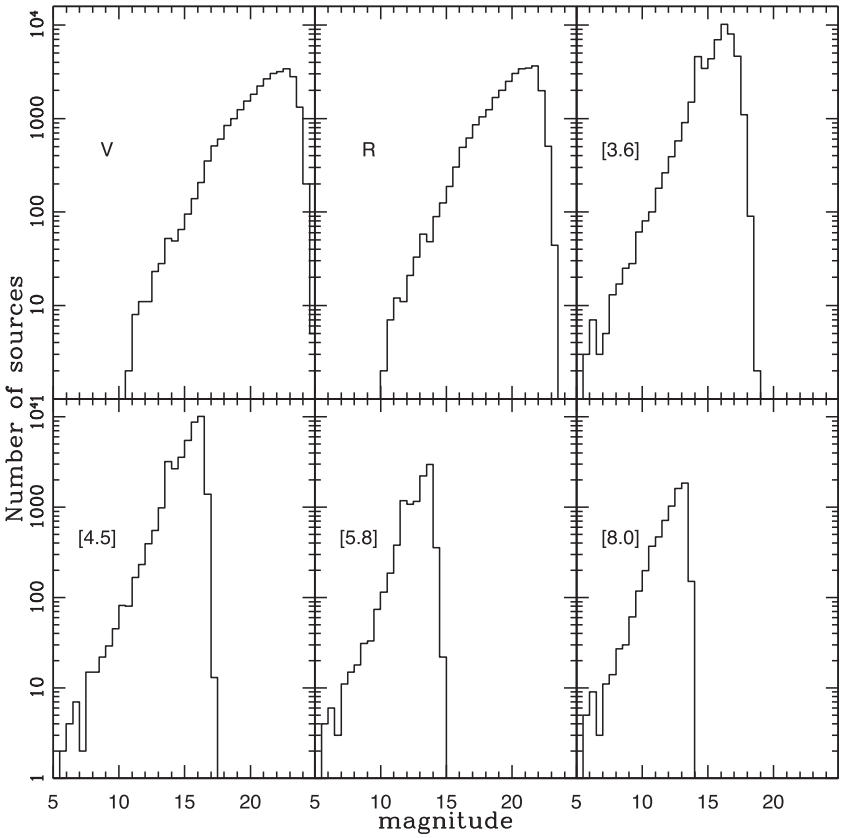

Figure 4. Histograms for the sources detected in optical and IRAC bands showing the limiting magnitude and completeness limit for each band.

Table 2. Completeness limit of the data in IRAC and optical bands.

Wavebands	*V*	*R*	[3.6]	[4.5]	[5.8]	[8.0]
Completeness (in mag)	22.5	22	16	16	14	13.5

colours suffers from the significant saturation in the IRAC 8 μm and MIPS 24 μm images caused by the central luminous sources as well as the bright nebulosity. Similarly, the variable reddening and stellar crowding characteristics across the region could also affect the local completeness limit. All these effects are difficult to quantify. Since 3.6 and 4.5 μm bands are the most commonly used colour combination for identifying Class II YSOs, we calculate the approximate completeness limit of our Class II YSOs by using the completeness limit of these two bands. The 90 per cent photometry completeness limits of 3.6 and 4.5 μm bands are estimated to be ∼16 mag. Assuming a distance of 2.0 kpc for IC 1805 and an average extinction A_v of ∼2.5 mag, we find that the photometric completeness limit corresponds to an approximate stellar mass in the range 0.2–0.3 $M_\odot$ for a YSO of age ∼2–3 Myr (using the evolutionary tracks of Siess, Dufour & Forestini 2000). The identification of Class III sources in our sample is primarily based on their detection in both the X-ray and optical bands. Only 62 per cent of the X-ray sources have optical counterparts. This indicates that the completeness limit of Class III YSOs is primarily dictated by the sensitivity limit of the optical data. The 90 per cent photometry completeness limits of the *V* and *R* bands lead to the completeness limit of our Class III YSOs as ∼0.3 $M_\odot$ at the assumed distance, mean A_v and age ∼2.5 Myr (using the evolutionary tracks of Siess et al. 2000). Adopting different sets of evolutionary tracks would provide different values of stellar masses. However, for low-mass objects, the tracks of Siess et al. (2000) are close to those of Baraffe et al. (1998). The agreement between masses of these two models is within 10–20 per cent. In summary, we considered that our YSO sample is expected to be largely complete above 0.3 $M_\odot$.

In the case of IC 1795, based on Franceschini et al. (2006) measurements from the IRAC/GOODS sample, Roccatagliata et al. (2011) calculated that the contamination of extragalactic sources in IRAC data is about 72 sources down to 15.5 mag at 3.6 μm for an area 0.°26 × 0.°26. IC 1805 is at the same distance and is associated with the same cloud complex as IC 1795, so a similar fraction of extragalactic contamination is expected in our IRAC catalogue. Scaling their values to our cluster area (i.e. the region covered by most of our observations; see Section 3.1.6), we expect ∼20 extragalactic IRAC sources. In addition to these, other contaminants such as broad-line AGNs, unresolved knots of shock emission and faint sources contaminated by copious PAH nebulosity (expected to be prevalent in distant massive star-forming regions) are also likely to affect our YSO selection. Using the criteria of Gutermuth et al. (2009), we have removed these contaminants from our catalogue. Although Gutermuth et al. (2009) criteria for a region at ∼2 kpc may provide an overestimation of the contamination, but this would ensure the high reliability of our YSO sample. Our X-ray YSO sample is selected based on the X-ray and optical observations. The majority of the extragalactic contaminants and distant background stars are expected not to have optical (*V*-band) counterparts. Moreover, optical images being at high spatial resolution and with our PSF photometry, extended objects like galaxies are unlikely to be the major contaminants in our sample. In the optical CMD, most of the likely members are located in the PMS zone and there are ∼40

Table 3. YSOs from 2MASS, IRAC/MIPS and X-ray data for the cluster area. The entire table is available in an electronic form.

Id	RA (J2000)	DEC (J2000)	$J\pm eJ$	$H\pm eH$	$K_s\pm eK_s$	[3.6]± e[3.6]	[4.5]± e[4.5]	[5.8]± e[5.8]	[8.0]± e[8.0]	[24]± e[24]
1	38.240929	61.374401	13.63 ± 0.04	12.65 ± 0.02	11.99 ± 0.02	12.38 ± 0.01	10.34 ± 0.01	9.58 ± 0.01	8.57 ± 0.01	6.94 ± 0.02
2	38.182259	61.469330	12.15 ± 0.02	11.65 ± 0.04	11.02 ± 0.03	9.58 ± 0.01	8.88 ± 0.01	8.03 ± 0.01	6.72 ± 0.01	4.15 ± 0.01
3	38.464951	61.406620	14.31 ± 0.04	13.88 ± 0.05	13.65 ± 0.04	13.61 ± 0.01	13.39 ± 0.01	13.02 ± 0.02	12.48 ± 0.03	–
.	.....	.....	.....	.....	.....	.....	.....	.....	.....	....

X-ray sources located near the MS. As discussed in Section 3.1.4, these sources are likely foreground sources of the region, and seem to agree well with the expected contamination in the direction of IC 1805. So overall, we expect that the likely number of X-ray contaminants in our YSO sample should be low.

3.1.6 Final catalogue of YSOs

Our final catalogue includes the YSO candidates identified from *Spitzer* IRAC/MIPS, 2MASS and X-ray data sets. In total, we have 297 Class III, eight transition disc and 272 Class I/II candidates in the direction of the W4 complex. However, there are only 101 Class I/II and 283 Class III candidates in the cluster (i.e. within ∼9 arcmin; see Section 3.2.1). The cluster radius is well within the common area covered by the X-ray, IRAC-MIPS as well as optical observations and our main aim is to explore and characterize the young stellar population associated with the cluster IC 1805. To determine the cluster properties, such as age (see Section 3.2.2), MF, disc-fraction and disc evolution of YSOs (discussed in Sections 4.1,4.2 and 4.3), we have used YSOs within the cluster radius, whereas to get an idea on the large scale star formation history, we have used all the YSOs identified in this work (discussed in Section 4.4). A sample list of the YSO candidates with their magnitudes in different bands for the cluster area is given in Table 3. The entire table is available in electronic form only.

In the W4 complex, using Bayes classifier and combining several criteria in a probabilistic approach, Broos et al. (2013) defined the list of MYStIX Probable Complex Members. Within 9 arcmin of the cluster centre, Broos et al. (2013) identified 389 YSOs (Xcl flag=2). Although a direct comparison with Broos et al. (2013) is not possible because of different methods used to extract photometric magnitudes on the *Spitzer* images (aperture photometry by them versus PRF photometry by us), and in the approach of YSO classification and contamination removal (for details see Broos et al. 2013). None the less, we find reasonable agreement between both the works. For example, within the cluster area we obtained 384 sources, whereas Broos et al. (2013) have identified 389 sources and only ∼15 per cent sources are missing in either of the catalogue.

In this work, we are more interested in studying the optical properties of the YSOs associated with the cluster. Unlike, NIR colours, the optical filters are more sensitive to the temperatures of late-type stars. Thus, in the low-extincted regions like IC 1805, the optical CMDs are expected to be more reliable in separating PMS members from the field stars and also better for the characterization of YSOs.

3.2 Properties of the cluster IC 1805

3.2.1 Physical extent of the cluster

The radial extent is one of the important parameters to study the dynamical properties of clusters. To estimate the cluster radius of IC 1805, we applied the star count technique and assumed a spherically symmetric distribution of stars in the cluster.

The point of maximum stellar density (α_{2000} = $02^h32^m42^s$; δ_{2000} = $+61^\circ27'21''$) taken from the WEBDA[3] is considered as the centre of IC 1805. It is worthy to mention that the adopted cluster centre is very close to the location of most massive star of the region (see Section 4.3). We then created the radial density profile (RDP) using our YSO catalogue to study the radial structure of the cluster. We divided the region into a number of concentric circles. The projected stellar density in each concentric annulus was obtained by dividing the number of stars by the respective annular area. The densities thus obtained are plotted as a function of radius in Fig. 5. The error bars are derived by assuming Poisson statistics. From the RDP, the cluster radius appears to be ∼9 arcmin (5 pc).

For comparison, we also estimated the extent of the cluster (r_{cl}) using 2MASS data. Within uncertainties, the r_{cl} obtained from the YSO sample and 2MASS data are matching. The RDP is parametrized with the empirical model of King (1962),

$$\rho(r) \propto \frac{\rho_0}{1+\left(\frac{r}{r_c}\right)^2},$$

where r_c is the core radius at which the surface density $\rho(r)$ becomes half of the central density, ρ_0. The best fit (solid line) to the radial density obtained by a χ^2 minimization technique is shown in Fig. 5.

3.2.2 CMD of YSOs: age and mass estimation

The ages and masses of the cluster members were estimated by comparing their locations on the CMD with PMS isochrones of various ages after correcting for the distance and extinction. The minimal differential extinction ($\Delta A_v \sim 0.6$ mag) towards the cluster is an advantage to examine the position of the YSOs on the CMD in order to confirm their youth, to determine their optical properties and to study the star formation history of the region.

Fig. 6 shows V versus $(V-R)$ CMD for the YSOs in the cluster area. The MS from Girardi et al. (2002) as well as the PMS isochrones for 1, 5 and 10 Myr for the solar metallicity from Siess et al. (2000), corrected for the adopted distance and reddening are also overplotted. The Class I and Class II sources (squares and diamonds, respectively) within the cluster area are identified based on the *Spitzer* IRAC/MIPS photometry. The location of X-ray emitting (likely Class III) sources is shown with the crosses. The age distribution of the majority of these sources is in the range of 0.5–7 Myr, concentrated around an age in the range of 2–3 Myr (mean age 2.5 ± 1.5 Myr). We find that masses for a majority of the YSOs are in the range of 0.2–2.5 $M_\odot$. As discussed in Section 3.1.4, our approach to select the Class III candidates might have removed some

[3] https://www.univie.ac.at/webda/

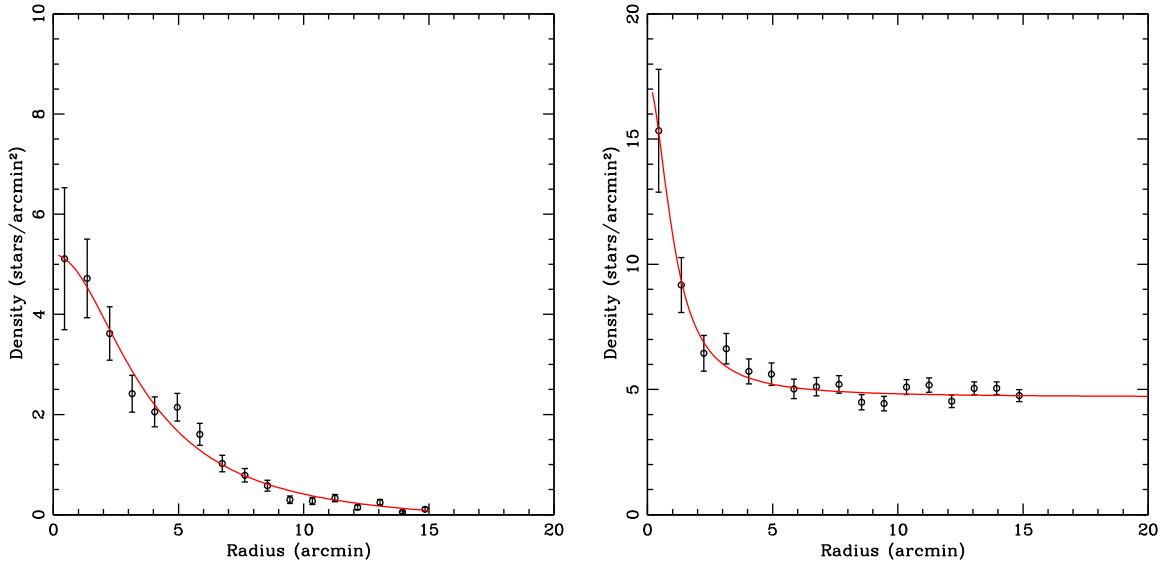

Figure 5. Radial density profile of the cluster IC 1805 based on the YSO sample (left-hand panel) and 2MASS data (right-hand panel). The continuous curve shows the least-squares fit of the King (1962) profile to the observed data points. The error bars represent $\pm\sqrt{N}$ errors.

YSOs, which may affect the mean age of the cluster. Hence, we also estimated the age of the cluster using only the disc-bearing sources (i.e. sources that have shown excess emission in the 2MASS and IRAC bands). This method resulted an age ∼2.3 Myr for the cluster, which is comparable to the mean age estimated using all the YSOs.

Age spread is common in young clusters and is probably due to the combined effect of differential reddening, circumstellar extinction, variability, binarity and/or different evolutionary stages (Jose et al. 2017). However, the reddening vector is nearly parallel to the isochrones, hence differential reddening does not have much effect on the age estimation of YSOs. The circumstellar extinction may affect the age and mass determination of Class 0/I sources, but its effect should be minimal in optically visible PMS sources such as Class III YSOs. Though the exact role of circumstellar discs requires detailed SED modelling or spectroscopic observations, which is beyond the scope of this paper, it is worthy to mention that Jose et al. (2013) performed SED modelling on a set of optically visible PMS sources and found that SED-based ages are largely in agreement with those estimated from the optical CMDs. A binary companion will apparently brighten the star, consequently CMD will yield a younger age. For example, in the case of equal-mass binaries, the cluster is expected to show a sequence in the CMD which is shifted by 0.75 mag upwards. The effect of binarity can be seen more prominently in some older clusters (∼10 Myr) for which the isochrones are close together (e.g. NGC 7160; Sicilia-Aguilar et al. 2005), whereas in the case of young clusters like Tr 37 (∼4 Myr), which is similar to IC 1805, the isochrones are well separated, hence the effect of binarity on age estimation will be less compared to the natural age spread of the stars in clusters (see discussion in Sicilia-Aguilar et al. 2005). Similarly, though T Tauri stars (TTSs) tend to show variability at optical bands (e.g. Herbst et al. 1994; Briceño et al. 2001; Rodríguez-Ledesma, Mundt & Eislöffel 2010; Lata et al. 2016), the variability tends to move the objects parallel to the isochrones, resulting in little effect on the age estimation of YSOs (Burningham et al. 2005). Despite low differential reddening and the presence of a large number of disc-less sources in the cluster, some degree of age spread due to the combination of the above factors is expected, but since the observed

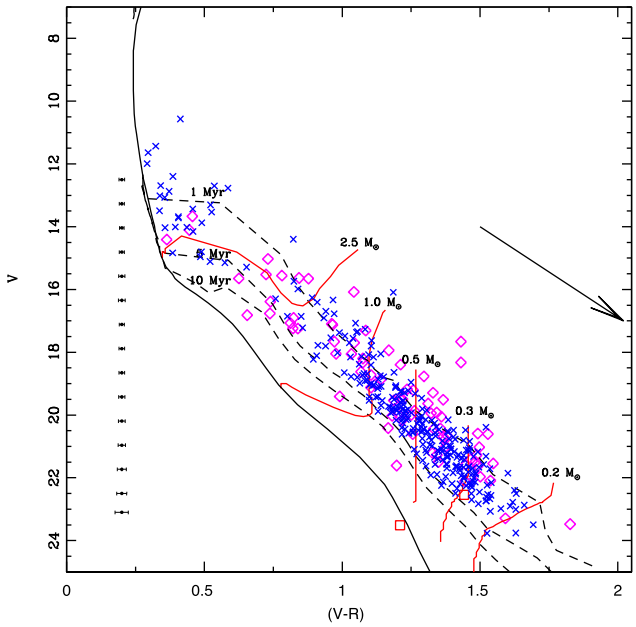

Figure 6. $V/(V-R)$ CMD for the YSO candidates in the cluster region. The PMS isochrones from Siess et al. (2000) and MS from Girardi et al. (2002), corrected for the adopted distance and reddening are also overplotted. The arrow is a reddening vector corresponding to $A_v = 3$ mag. Diamonds and squares represent the Class II and Class I sources, respectively. Blue crosses represent the X-ray sources that are considered as YSOs (see Sections 3.1.4 and 3.2.2) in this study.

spread in colour due to member YSOs is larger than their mean uncertainties due to photometric colours (see Fig. 6), we expect that the YSOs are at different evolutionary stages.

We considered that the errors associated with the determination of age and mass are mainly of two kinds; random errors in photometry and systematic errors due to different theoretical evolutionary tracks. We estimated the effect of random errors by propagating them to the observed estimations of V, $(V-R)$ and $E(V-R)$

Table 4. Magnitudes, age and mass of the YSOs in the cluster region. Complete table is available in an electronic form.

Id	RA (J2000)	DEC (J2000)	$V \pm eV$	$R \pm eR$	Age ± error in age (Myr)	Mass ± error in mass ($M_\odot$)
1	37.888229	61.429279	22.10 ± 0.02	20.66 ± 0.01	3.01 ± 0.65	0.31 ± 0.02
2	37.895050	61.506271	21.28 ± 0.01	19.79 ± 0.01	1.20 ± 0.30	0.30 ± 0.02
3	37.919338	61.502380	19.87 ± 0.01	18.61 ± 0.01	1.57 ± 0.57	0.57 ± 0.08
...	...	...	...	...		

by assuming a normal error distribution and using Monte Carlo simulations (see e.g. Chauhan et al. 2009). Since we have used the evolutionary model by Siess et al. (2000) for all the PMS stars, the age and mass estimations given in Table 4 should not be affected by systematic errors. A sample of Table 4 is given here and the complete table is available in the electronic version.

4 DISCUSSION

4.1 MF of the YSOs

Young clusters are the best objects to study the initial MFs. Since young low-mass stars have limited time to segregate from the cluster and/or loose mass through evolutionary processes, the variation of the MF gives clues about the physical conditions of the star formation process. The MF is defined as the number of stars per unit logarithmic mass interval, and is generally represented by a power law with a slope,

$\Gamma = \mathrm{d} \log N(\log m)/\mathrm{d} \log m,$

where $N(\log m)$ is the distribution of the number of stars per unit logarithmic mass interval. Most of the star clusters in the solar neighbourhood have MF slopes near the Salpeter MF slope, that is,

$\Gamma = -1.35.$

Since our YSO sample is complete down to 0.3 $M_\odot$, for the MF study we have taken only those YSOs that have masses in the range $0.3 \leq M/M_\odot \leq 2.5$. The mass distribution of our YSO sample has a best-fitting slope, $\Gamma = -1.23 \pm 0.14$ (see Fig. 7). Ninkov et al. (1995) studied the cluster IC 1805 and found a slope of $\Gamma = -1.38 \pm 0.19$ for masses between 2.5 and 30 $M_\odot$. A similar value of Γ ($= -1.3 \pm 0.2$) has been reported by Massey et al. (1995) for the massive stars of the W4 complex. Our YSO MF is consistent with those reported for other active star-forming regions. Erickson et al. (2011) derived the MF of an extinction-limited YSO sample (with masses >0.2 $M_\odot$) consistent with the field star MF. Kang et al. (2009) did not find any difference in the YSO MF slopes of the star-forming regions W51 A ($\Gamma = -1.17 \pm 0.26$) and W51 B ($\Gamma = -1.32 \pm 0.26$). We note that a few older Class III sources might have been excluded as contaminants due to our conservative selection criteria (see Section 3.1.4). Even then, we believe our result should represent the IMF for the cluster, for example, and low-mass isochrones are very close to each other.

4.2 Evolution of T-Tauri stars in IC 1805

TTSs are low-mass stars (< 3 $M_\odot$) that are contracting towards the MS. They are generally classified into weak-line TTSs (WTTSs) and classical TTSs (CTTSs) on the basis of the strength of the Hα emission line (Strom et al. 1989). WTTSs exhibit a weak, narrow Hα (EW $\leq$ 10 Å) in emission with no or little IR excess, while CTTSs display a strong Hα emission line (EW $\geq$ 10 Å) and large IR excesses. Class II sources are generally considered to correspond in the optical category to CTTSs and Class III sources to WTTSs

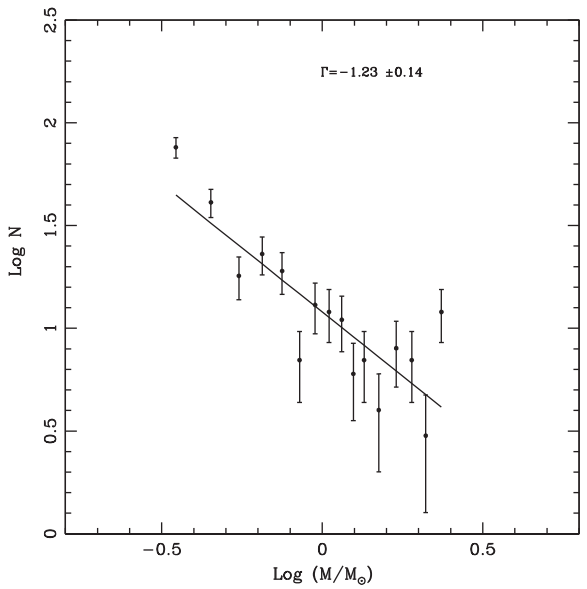

Figure 7. The MF of the candidate YSOs in the mass range ($0.3 \leq M/M_\odot \leq 2.5$), derived from the optical data. The error bars represent $\pm \sqrt{N}$ errors. The continuous line shows the least-squares fit to the mass ranges described in the text. The value of the slope obtained is given in the figure.

(e.g. Hartmann et al. 2005; Pandey et al. 2013a). The 'standard model' by Kenyon & Hartmann (1995) postulates that the CTTSs evolve to WTTSs by losing their circumstellar discs or at least their inner parts. In the Taurus region, the WTTSs are systematically older than the CTTSs (Bertout, Siess & Cabrit 2007), but the statistical significance is low (Kenyon & Hartmann 1995; Hartmann 2001; Armitage, Clarke & Palla 2003). Contrary to the above results, there are studies which favour the assumption that CTTS and WTTS are coeval and possess indistinguishable stellar properties (Lawson, Feigelson & Huenemoerder 1996; Gras-Velázquez & Ray 2005). The coevality of CTTSs and WTTSs in a star-forming region can be explained by assuming that YSOs have intrinsically a wide range of disc masses and their accretion activity and/or the dispersal of the disc takes place in a correspondingly wide range of time-scales (Furlan et al. 2006; Bertout et al. 2007).

In this work, we have derived the ages of a large sample of YSOs in the IC 1805 cluster, hence, it is worth to attempt to address the problem of the evolutionary status of CTTSs and WTTSs. Fig. 8(a) shows the histograms of the ages of the CTTS and WTTS candidates within the cluster region in the mass range 0.3–2.5 $M_\odot$. This manifests that the CTTSs are relatively younger (mean age ~2.3 Myr) than the WTTSs (mean age ~2.6 Myr). The cumulative distribution of the ages of CTTSs and WTTSs is shown in Fig. 8(b). We obtained the Kolmogorov–Smirnov test value of 11 per cent for the assumption that the two samples drawn are from the same population. Although the statistical significance is less, our result is in agreement with those of Bertout et al. (2007) for the Taurus–Auriga

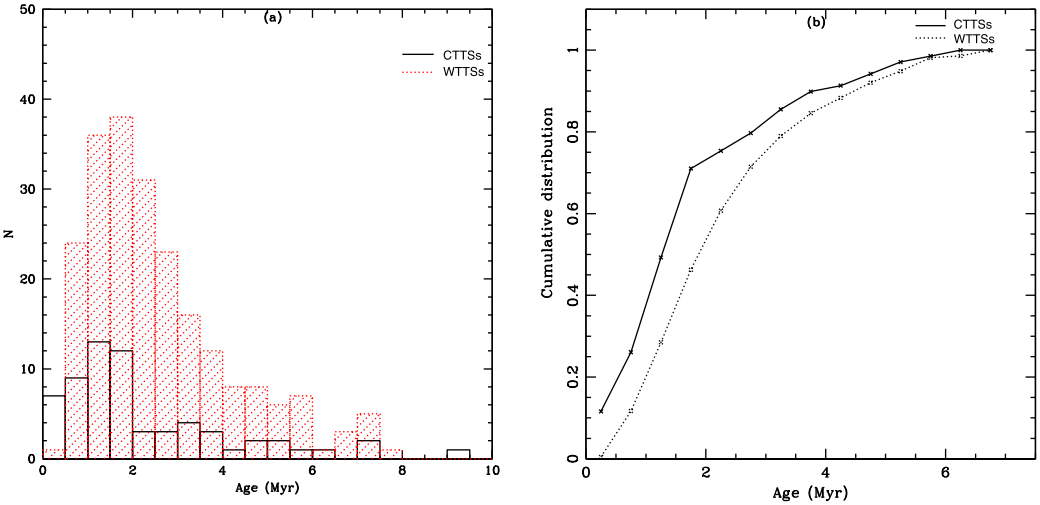

Figure 8. (a) Histograms of the age distribution of the Class II and Class III candidates, (b) cumulative distributions of CTTSs and WTTSs in the cluster region as a function of stellar age.

T-association and of Chauhan et al. (2009) for the BRC regions, that WTTSs are relatively older than CTTSs, which supports the notion that CTTSs evolve into WTTSs. Here again, we would like to remind readers that these results are affected by the uncertainty associated with the membership of the stars (see Section 3.1.4), particularly the WTTSs (spectroscopic information is needed to confirm the true nature of WTTSs and CTTSs).

4.3 Disc fraction variation in the cluster

The disc fraction of YSOs in clusters decreases with ages (e.g. Haisch, Lada & Lada 2001; Hernández et al. 2008). Haisch et al. (2001) quantitatively concluded that in young clusters an initially very high (80–90 per cent) disc fraction decreases to 50 per cent in ∼3 Myr and reaches almost 10 per cent at ∼5 Myr. Generally, massive stars seem to lose their discs earlier than lower mass stars. For example, most low-mass stars (spectral type K5 and later) lose their discs in 5–7 Myr (e.g. Sicilia-Aguilar et al. 2005), whereas for the intermediate-mass Herbig Ae/Be stars the corresponding time-scale is <3 Myr (e.g. Hernández et al. 2005).

In a young cluster, the disc fraction depends also on the spatial position. Theoretical calculations predict that external UV radiation of high-mass stars can photoevaporate outer discs only within 0.3–0.7 pc (Johnstone, Hollenbach & Bally 1998; Adams et al. 2004). A decrease in disc frequencies in the immediate vicinity of massive stars has been found in several massive clusters, e.g. NGC 2244, NGC 6611 and Pismis 24 (Balog et al. 2007; Mercer et al. 2009; Fang et al. 2012), suggesting rapid destruction of circumstellar discs in such environments. IC 1805 is a young cluster (age ∼2.5 Myr) with several low-mass (<2.5 $M_{\odot}$) stars that have discs, thus the cluster represents a good site for studying the influence of massive stars on the evolution of discs.

In IC 1805, it is argued that the region is mainly powered by three O-type stars (Lefloch et al. 1997). BD +60502 and BD +60501 are of the spectral type O4.5III (Sota et al. 2014) and O7V (Sota et al. 2011), respectively, and are located near the assumed cluster centre (see Fig. 9), whereas HD 15570 is an O4I star (Sota et al. 2011), located ∼4.7 arcmin east of the cluster centre. The radial velocities of BD +60502 and BD +60501 are −42 km s^{-1} (Kharchenko et al. 2007) and −52 km s^{-1} (Kharchenko et al. 2007), respectively, consistent with the molecular cloud velocity (−55 to

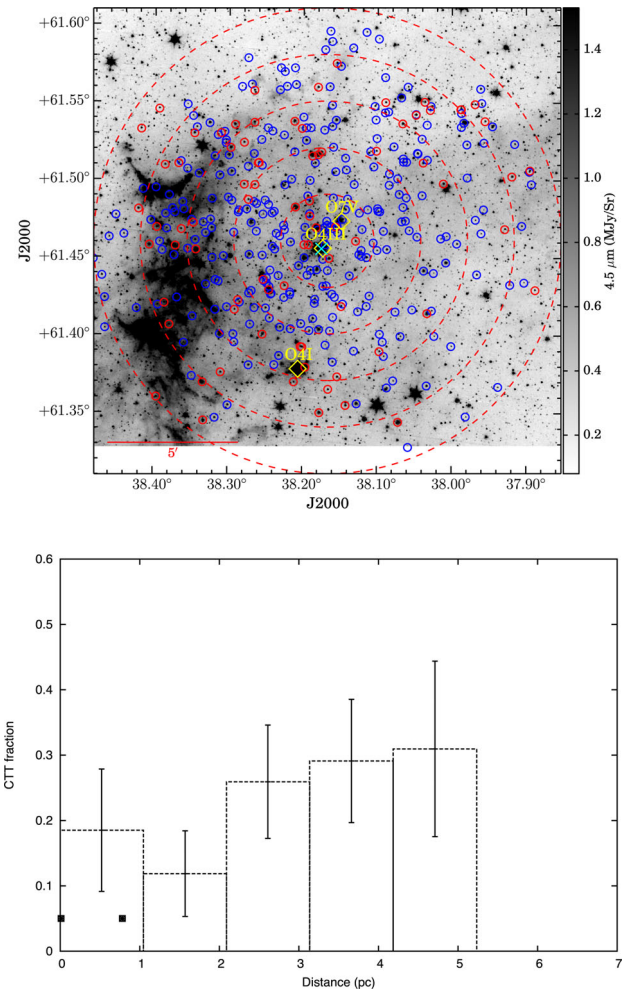

Figure 9. The upper panel shows the surface distribution of WTTSs (blue circles) and CTTSs (red circles) superposed on the *Spitzer* 4.5 μm image of the cluster. The concentric annuli have a width of 1.8 arcmin. The massive stars are shown with diamond symbols and cluster centre with cross. The lower panel shows the CTTS fraction as a function of the radial distance from the cluster centre. The two filled squares represent the locations of the two massive stars near the cluster centre.

-32 km s^{-1}) associated with the W3/W4 complex (Heyer & Terebey 1998). The radial velocity of HD 15570 is -24.00 km s^{-1} (Gontcharov 2006), thus to unlikely belong to the W3/W4 complex, but seems consistent with that of an object in an interarm cloud, whose velocity lies between -32 and -18 km s^{-1} (Heyer & Terebey 1998). We conclude that the cluster is dominated by the O4.5III and O7V stars located near the cluster centre.

To study the influence of these massive stars on the evolution of nearby low-mass stars, we divided the cluster area into five concentric annuli (each of width 1.8 arcmin). Fig. 9 (upper panel) displays the distribution of CTTSs (red circles) and WTTSs (blue circles) in the mass range 0.3–2.5 $M_{\odot}$ from the catalogue of YSOs for which we have mass estimations from the optical CMDs. Our aim is to examine the disc fraction variation of the low-mass stars within the cluster due to external influence, as massive stars can self-destroy their disc, because evolution of protoplanetary discs is faster around higher mass stars (e.g. Kennedy & Kenyon 2009; Yasui et al. 2014). Fig. 9 (lower panel) displays the fraction of low-mass CTTSs (i.e. the ratio between CTTSs and CTTSs+WTTSs in each annular area) as a function of the projected radial distance from the cluster centre which is only 0.03 pc away from BD +60502. In the figure, the substantial uncertainties shown as solid lines originate from the low statistics of IR excess sources in each bin. We also checked the distribution of disc frequency by recentring the analysis on the O7 star and find the disc frequency variation to be nearly the same. Although we see a dip in the disc-fraction versus distance plot in the vicinity of the O-type star, due to large statistical error, we do not have a strong evidence of variation in the disc fraction within the cluster. However, we note that the disc fraction estimation can be affected by many factors, such as various methods used to identify YSOs, the variation in stellar density (e.g. Spezzi et al. 2015), sensitivity of different bands and the uncertainty in the membership of the older WTTs. For example, *Spitzer* observations of high-mass star-forming regions suffer from high, non-uniform nebulosity, primarily emission from PAHs at IRAC bands and is strong close to the massive stars near the centre of rich clusters, where stellar crowding is high. In contrast, *Chandra*'s sensitivity is less affected by nebulosity and moreover it has several times better on-axis spatial resolution than *Spitzer*. So IRAC bands can lead to severe decrease in sensitivity of the disc-bearing YSOs compared to disc-less YSOs near the cluster centre. None the less, our result is in agreement with Roccatagliata et al. (2011), who found no variation of the disc fraction as a function of the distance from the high-mass stars in IC 1795, which has a similar number of high mass stars and located in the same cloud complex.

4.4 Star formation history

Fig. 10 shows the Canadian Galactic Plane Survey (CGPS; Taylor et al. 2003) 1.4 GHz emission in the direction of the W4 bubble, superimposed on the *WISE*[4] 12 μm emission and *Herschel*[5] in 250 μm emission. We have also marked the BRCs in the region (Sugitani et al. 1991). The 12 μm *WISE* band contains 11.7 μm emission commonly attributed to PAH molecules excited in the photon-dominated regions (PDRs) at the interface of H II regions and their adjacent molecular clouds by the far-UV photons leaking from the H II regions (Pomarès et al. 2009). Therefore, PAHs are

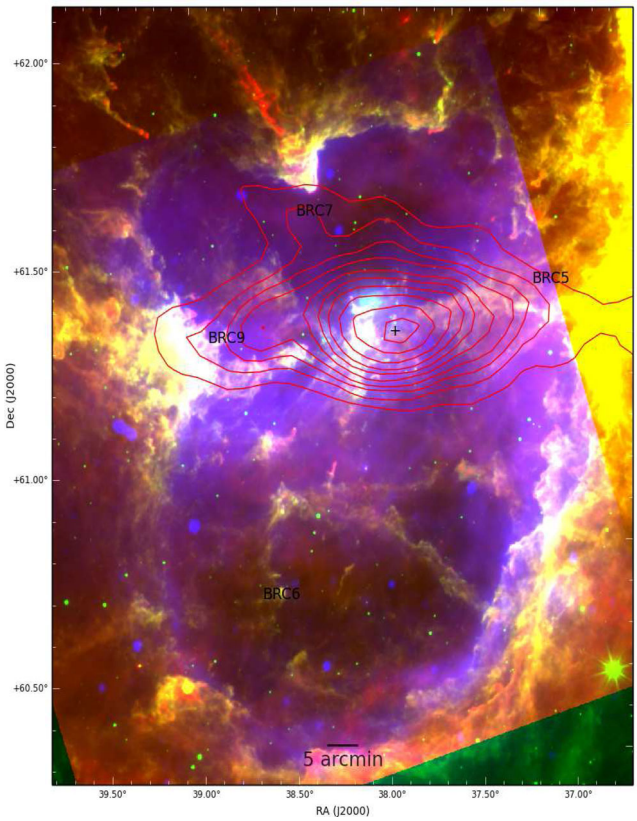

Figure 10. Colour composite image of the IC 1805 region reproduced with CGPS 1.4 GHz emission (blue colour) superimposed on those of the *WISE* 12 μm emission (green colour) and *Herschel* 250 μm emission (red colour). BRCs associated with the region and catalogued in Sugitani et al. (1991) are also marked in the figure. The red contours display the surface density distribution of the YSOs with the plus symbol representing the cluster centre.

good tracers of the warm PDR that surrounds the H II region. PAH emission is also a good tracer of newly formed, embedded B-type star formation (Peeters, Spoon & Tielens 2004), as these stars heat the surrounding dust to high temperatures enough to excite the PAH bands and fine-structure lines. Fig. 10 reveals a filamentary distribution of the 12 μm emission with its long axis in the east–west direction that bisects the H II region and also in the PDRs at the periphery of the bubble. The dust emission detected by the *Herschel* 250 μm also has an elongated distribution similar to that of the 12 μm emission. Compared to the PAH and dust emission, the ionized gas appears to be distributed orthogonal to the long axis of the filamentary structure, with decreasing intensity away from the filament axis. The ionized gas seems to be bounded more towards the east and west directions than in the north and south. The overall morphology of the nebula looks bipolar. Such a bipolar morphology has been noticed in NIR to MIR bands in a few H II regions and/or bubbles (see e.g. Saito et al. 2009; Deharveng et al. 2012; Samal et al. 2012; Mallick et al. 2013). Recently, *Herschel* observations have clearly shown the presence of a cold dense neutral filament in bipolar H II regions that bisects ionized lobes (e.g. Deharveng et al. 2015), similar to the one observed here. Thus, the elongated nature of the 250 μm emission most likely represents the long axis of the parental filament.

It has been suggested that the stellar distribution in star-forming regions is governed by the structure of the parental molecular cloud

[4] http://irsa.ipac.caltech.edu/applications/wise/
[5] http://www.cosmos.esa.int/web/herschel/science-archive/

as well as how star formation proceeds in the cloud (e.g. Chen, Chen & Shu 2004; Sharma et al. 2006; Schmeja, Kumar & Ferreira 2008; Gutermuth et al. 2009; Samal et al. 2015; Jose et al. 2016). Although our survey does not sample all the YSOs of the W4 complex, it is good enough to provide clues on the star formation history. We generated the YSO stellar surface density map using the nearest neighbourhood method (Gutermuth et al. 2005). At each sample position $[i, j]$ in a uniform grid, we measured $r_N(i, j)$, the projected radial distance to the Nth nearest star. The value of N is allowed to vary depending upon the desired smallest scale structures of interest. We generated a map using $N = 20$, which, after a series of experiments, was obtained as a good compromise between the resolution and signal-to-noise ratio of the map. In the stellar surface density distribution (see Fig. 10), the YSOs show a centrally concentrated clustering. At the same time, the overall distribution has an elongation along the east–west direction, following the structure revealed by the 250 μm emission. Thus, it appears that the formation of the cluster IC 1805 possibly started in a filamentary cloud, where the density was high along the axis of the filament and low towards the perpendicular directions. With time the O stars of the cluster developed an H II region, which subsequently grew in size, first inside the dense filament, then opening out in a hole in the low-density direction of the filament, resulting a large cavity in the north and south direction. Based on the distribution of young stars on the *Herschel* images, Deharveng et al. (2012) have suggested that young clusters in the W5 complex were also formed in a filamentary cloud. In the W4 complex, we could see a few BRC structures in the north and south directions facing the IC 1805 cluster (see Fig. 10). This could be due to the fact that as the ionized gas streams away in the low-density side, it encounters a few small, dense clouds along its way, forming the BRC structures.

The YSO distribution along the filament axis of the W4 bubble suggests that some of them could have resulted from the fragmentation of the original filament as are the cases found in other filamentary systems (e.g. Jackson et al. 2010; Hacar & Tafalla 2011; Samal et al. 2015) and/or due to compression of dense gas of the primordial filament by an expanding H II region. Though precise characterization (e.g. proper motion and age) of individual YSOs projected on the filament is needed to understand their origin, the overall morphology of the W4 H II region and the distribution of the associated YSOs suggest that IC 1805 could have been formed in a filamentary cloud.

5 CONCLUSIONS

With the aim of unravelling the less known low-mass YSO population of the cluster IC 1805 which is rich in massive OB stars, we studied the region using optical, IR and X-ray data sets. Our results suggest that despite the less favourable conditions for star formation around the high-mass stars, IC 1805 shows signs of low-mass star formation similar to other clusters in the solar vicinity. We identified and characterized a large number of low-mass YSO candidates in the region. Most of them have masses in the range 0.2–2.5 $M_\odot$ and age 0.1–5 Myr. The slope of the MF in the mass range $0.3 \leq M/M_\odot \leq 2.5$ is found to be $\Gamma = -1.23 \pm 0.14$, similar to the Salpeter MF. The mean age of the candidate YSOs is found to be ∼2.5 Myr. The candidate WTTSs are found to be relatively older when compared to the CTTS candidates. We do not find strong evidence for disc dispersal due to massive stars. The spatial distribution of the YSOs, dust and gas in the H II complex shows a filamentary distribution, which suggests the filamentary morphology of the parental molecular cloud.

ACKNOWLEDGEMENTS

We are thankful to the anonymous referee for valuable comments. NP acknowledges financial support from the Department of Science and Technology, INDIA, through INSPIRE faculty award IFA12-PH-36 at University of Delhi. The work at NCU is supported by the National Science Council through the grant no. 102-2119-M-008-001. This publication makes use of data from the Two Micron All Sky Survey (a joint project of the University of Massachusetts and the Infrared Processing and Analysis Center/California Institute of Technology, funded by the National Aeronautics and Space Administration and the National Science Foundation), archival data obtained with the *Spitzer Space Telescope* (operated by the Jet Propulsion Laboratory, California Institute of Technology, under contract with the NASA), and data products from the Wide-field Infrared Survey Explorer, which is a joint project of the University of California, and the Jet Propulsion Laboratory/California Institute of Technology, funded by the NASA. Herschel is an ESA space observatory with science instruments provided by European-led Principal Investigator consortia and with important participation from NASA. This research used the facilities of the Canadian Astronomy Data Centre operated by the National Research Council of Canada with the support of the Canadian Space Agency.

REFERENCES

Adams F. C., Lada C. J., Shu F. H., 1987, ApJ, 312, 788
Adams F. C., Hollenbach D., Laughlin G., Gorti U., 2004, ApJ, 611, 360
Allen L. E. et al., 2004, ApJS, 154, 363
Allen L. et al., 2007, Protostars and Planets V. Univ. Arizona Press, AZ, Tucson, p. 361
Allen T. S. et al., 2012, ApJ, 750, 125
André P., 1995, Ap&SS, 224, 29
André P., Ward-Thompson D., Barsony M., 1993, ApJ, 406, 122
Armitage P. J., Clarke C. J., Palla F., 2003, MNRAS, 342, 1139
Bally J., Sutherland R. S., Devine D., Johnstone D., 1998, AJ, 116, 293
Balog Z., Muzerolle J., Rieke G. H., Su K. Y. L., Young E. T., Megeath S. T., 2007, ApJ, 660, 1532
Baraffe I., Chabrier G., Allard F., Hauschildt P. H., 1998, A&A, 337, 403
Bertout C., Siess L., Cabrit S., 2007, A&A, 473, L21
Bisbas T. G., Wünsch R., Whitworth A. P., Hubber D. A., 2009, A&A, 497, 649
Briceño C. et al., 2001, Science, 291, 93
Broos P. S. et al., 2013, ApJS, 209, 32
Burningham B., Naylor T., Littlefair S. P., Jeffries R. D., 2005, MNRAS, 363, 1389
Carpenter J. M., Mamajek E. E., Hillenbrand L. A., Meyer M. R., 2006, ApJ, 651, L49
Chauhan N., Pandey A. K., Ogura K., Ojha D. K., Bhatt B. C., Ghosh S. K., Rawat P. S., 2009, MNRAS, 396, 964
Chauhan N., Pandey A. K., Ogura K., Jose J., Ojha D. K., Samal M. R., Mito H., 2011, MNRAS, 415, 1202
Chen W. P., Chen C. W., Shu C. G., 2004, AJ, 128, 2306
Cutri R. M. et al., 2003, 2MASS All Sky Catalog of point sources
Dahm S. E., Hillenbrand L. A., 2007, AJ, 133, 2072
Deharveng L. et al., 2010, A&A, 523, A6
Deharveng L. et al., 2012, A&A, 546, A74
Deharveng L. et al., 2015, A&A, 582, A1
Erickson K. L., Wilking B. A., Meyer M. R., Robinson J. G., Stephenson L. N., 2011, AJ, 142, 140
Evans N. J., II, et al., 2003, PASP, 115, 965
Fang M. et al., 2012, A&A, 539, A119
Fazio G. G. et al., 2004, ApJS, 154, 10
Feigelson E. D., Montmerle T., 1999, ARA&A, 37, 363
Flaherty K. M., Pipher J. L., Megeath S. T., Winston E. M., Gutermuth R. A., Muzerolle J., Allen L. E., Fazio G. G., 2007, ApJ, 663, 1069

Franceschini A. et al., 2006, A&A, 453, 397
Furlan E. et al., 2006, ApJS, 165, 568
Getman K. V., Feigelson E. D., Grosso N., McCaughrean M. J., Micela G., Broos P., Garmire G., Townsley L., 2005, ApJS, 160, 353
Getman K. V., Feigelson E. D., Townsley L., Broos P., Garmire G., Tsujimoto M., 2006, ApJS, 163, 306
Girardi L., Bertelli G., Bressan A., Chiosi C., Groenewegen M. A. T., Marigo P., Salasnich B., Weiss A., 2002, A&A, 391, 195
Gontcharov G. A., 2006, Astron. Lett., 32, 759
Gorti U., Hollenbach D., 2009, ApJ, 690, 1539
Goudis C., White N. J., 1980, A&A, 83, 79
Gras-Velázquez À., Ray T. P., 2005, A&A, 443, 541
Güdel M., Skinner S. L., Mel'Nikov S. Y., Audard M., Telleschi A., Briggs K. R., 2007, A&A, 468, 529
Guetter H. H., Vrba F. J., 1989, AJ, 98, 611
Gutermuth R. A., Megeath S. T., Pipher J. L., Williams J. P., Allen L. E., Myers P. C., Raines S. N., 2005, ApJ, 632, 397
Gutermuth R. A., Megeath S. T., Myers P. C., Allen L. E., Pipher J. L., Fazio G. G., 2009, ApJS, 184, 18
Hacar A., Tafalla M., 2011, A&A, 533, A34
Hachisuka K. et al., 2006, ApJ, 645, 337
Haisch K. E., Jr., Lada E. A., Lada C. J., 2001, AJ, 121, 2065
Hanson M. M., Clayton G. C., 1993, AJ, 106, 1947
Hartmann L., 2001, AJ, 121, 1030
Hartmann L., Megeath S. T., Allen L., Luhman K., Calvet N., D'Alessio P., Franco-Hernandez R., Fazio G., 2005, ApJ, 629, 881
Herbst W., Herbst D. K., Grossman E. J., Weinstein D., 1994, AJ, 108, 1906
Hernández J., Calvet N., Hartmann L., Briceño C., Sicilia-Aguilar A., Berlind P., 2005, AJ, 129, 856
Hernández J., Briceño C., Calvet N., Hartmann L., Muzerolle J., Quintero A., 2006, ApJ, 652, 472
Hernández J., Hartmann L., Calvet N., Jeffries R. D., Gutermuth R., Muzerolle J., Stauffer J., 2008, ApJ, 686, 1195
Heyer M. H., Terebey S., 1998, ApJ, 502, 265
Indebetouw R., Robitaille T. P., Whitney B. A., Churchwell E., Babler B., Meade M., Watson C., Wolfire M., 2007, ApJ, 666, 321
Jackson J. M., Finn S. C., Chambers E. T., Rathborne J. M., Simon R., 2010, ApJ, 719, L185
Johnstone D., Hollenbach D., Bally J., 1998, ApJ, 499, 758
Jose J. et al., 2013, MNRAS, 432, 3445
Jose J., Kim J. S., Herczeg G. J., Samal M. R., Bieging J. H., Meyer M. R., Sherry W. H., 2016, ApJ, 822, 49
Jose J., Herczeg G. J., Samal M. R., Fang Q., Panwar N., 2017, ApJ, 836, 98
Joshi U. C., Sagar R., 1983, J. R. Astron. Soc. Can., 77, 40
Kang M., Bieging J. H., Povich M. S., Lee Y., 2009, ApJ, 706, 83
Kennedy G. M., Kenyon S. J., 2009, ApJ, 695, 1210
Kenyon S. J., Hartmann L., 1995, ApJS, 101, 117
Kharchenko N. V., Scholz R.-D., Piskunov A. E., Röser S., Schilbach E., 2007, Astron. Nachr., 328, 889
King I., 1962, AJ, 67, 471
Koenig X. P., Allen L. E., Gutermuth R. A., Hora J. L., Brunt C. M., Muzerolle J., 2008, ApJ, 688, 1142
Koenig X. P., Leisawitz D. T., Benford D. J., Rebull L. M., Padgett D. L., Assef R. J., 2012, ApJ, 744, 130
Kroupa P., 2002, Science, 295, 82
Kwon S. M., Lee S.-W., 1983, J. Korean Astron. Soc., 16, 7
Lada C. J., 1987, in Peimbert M., Jugaku J., eds., Proc. IAU Symp. 115, Star Forming Regions. Reidel, Dordrecht, p. 1
Lada C. J., Lada E. A., 2003, ARA&A, 41, 57
Lada C. J., Elmegreen B. G., Cong H.-I., Thaddeus P., 1978, ApJ, 226, L39
Landolt A. U., 1992, AJ, 104, 340
Lata S., Pandey A. K., Panwar N., Chen W. P., Samal M. R., Pandey J. C., 2016, MNRAS, 456, 2505
Lawson W. A., Feigelson E. D., Huenemoerder D. P., 1996, MNRAS, 280, 1071
Lefloch B., Lazareff B., Castets A., 1997, A&A, 324, 249
Mallick K. K., Kumar M. S. N., Ojha D. K., Bachiller R., Samal M. R., Pirogov L., 2013, ApJ, 779, 113
Marino A., Micela G., Peres G., 2000, A&A, 353, 177
Massey P., Johnson K. E., Degioia-Eastwood K., 1995, ApJ, 454, 151
Megeath S. T. et al., 2004, ApJS, 154, 367
Megeath S. T. et al., 2012, AJ, 144, 192
Mercer E. P., Miller J. M., Calvet N., Hartmann L., Hernandez J., Sicilia-Aguilar A., Gutermuth R., 2009, AJ, 138, 7
Miao J., White G. J., Thompson M. A., Nelson R. P., 2009, ApJ, 692, 382
Muzerolle J. et al., 2006, ApJ, 643, 1003
Ninkov Z., Bretz D. R., Easton R. L., Jr, Shure M. A., 1995, AJ, 110, 2242
Oey M. S., Watson A. M., Kern K., Walth G. L., 2005, AJ, 129, 393
Ogura K., Sugitani K., Pickles A., 2002, AJ, 123, 2597
Ojha D. K. et al., 2011, ApJ, 738, 156
Pandey A. K., Samal M. R., Chauhan N., Eswaraiah C., Pandey J. C., Chen W. P., Ojha D. K., 2013a, New Astron., 19, 1
Pandey A. K. et al., 2013b, ApJ, 764, 172
Pandey A. K., Samal M. R., Yadav R. K., Richichi A., Lata S., Pandey J. C., Ojha D. K., Chen W. P., 2014, New Astron., 29, 18
Panwar N., Chen W. P., Pandey A. K., Samal M. R., Ogura K., Ojha D. K., Jose J., Bhatt B. C., 2014, MNRAS, 443, 1614
Peeters E., Spoon H. W. W., Tielens A. G. G. M., 2004, ApJ, 613, 986
Pomarès M. et al., 2009, A&A, 494, 987
Povich M. S. et al., 2009, ApJ, 696, 1278
Povich M. S. et al., 2013, ApJS, 209, 31
Preibisch T., Feigelson E. D., 2005, ApJS, 160, 390
Preibisch T., Brown A. G. A., Bridges T., Guenther E., Zinnecker H., 2002, AJ, 124, 404
Prisinzano L., Damiani F., Micela G., Sciortino S., 2005, A&A, 430, 941
Reach et al., 2005, PASP, 117, 978
Roccatagliata V., Bouwman J., Henning T., Gennaro M., Feigelson E., Kim J. S., Sicilia-Aguilar A., Lawson W. A., 2011, ApJ, 733, 113
Rodríguez-Ledesma M. V., Mundt R., Eislöffel J., 2010, A&A, 515, A13
Sagar R., 1987, MNRAS, 228, 483
Sagar R., Yu Q. Z., 1990, ApJ, 353, 174
Saito H. et al., 2009, AJ, 137, 3149
Samal M. R., Pandey A. K., Ojha D. K., Chauhan N., Jose J., Pandey B., 2012, ApJ, 755, 20
Samal M. R. et al., 2014, A&A, 566, A122
Samal M. R. et al., 2015, A&A, 581, A5
Schmeja S., Kumar M. S. N., Ferreira B., 2008, MNRAS, 389, 1209
Sharma S., Pandey A. K., Ogura K., Mito H., Tarusawa K., Sagar R., 2006, AJ, 132, 1669
Sicilia-Aguilar A., Hartmann L. W., Hernández J., Briceño C., Calvet N., 2005, AJ, 130, 188
Siess L., Dufour E., Forestini M., 2000, A&A, 358, 593
Sota A., Maíz Apellániz J., Walborn N. R., Alfaro E. J., Barbá R. H., Morrell N. I., Gamen R. C., Arias J. I., 2011, ApJS, 193, 24
Sota A., Maíz Apellániz J., Morrell N. I., Barbá R. H., Walborn N. R., Gamen R. C., Arias J. I., Alfaro E. J., 2014, ApJS, 211, 10
Spezzi L., Petr-Gotzens M. G., Alcalá J. M., Jørgensen J. K., Stanke T., Lombardi M., Alves J. F., 2015, A&A, 581, A140
Stetson P. B., 1987, PASP, 99, 191
Stetson P. B., 1992, J. R. Astron. Soc. Can., 86, 71
Straižys V., Boyle R. P., Janusz R., Laugalys V., Kazlauskas A., 2013, A&A, 554, A3
Strom K. M., Newton G., Strom S. E., Seaman R. L., Carrasco L., Cruz-Gonzalez I., Serrano A., Grasdalen G. L., 1989, ApJS, 71, 183
Sugitani K., Fukui Y., Ogura K., 1991, ApJS, 77, 59
Sung H., Bessell M. S., 2004, AJ, 127, 1014
Sung H., Lee S.-W., 1995, J. Korean Astron. Soc., 28, 119
Taylor A. R., Irwin J. A., Matthews H. E., Heyer M. H., 1999, ApJ, 513, 339
Taylor A. R. et al., 2003, AJ, 125, 3145
Townsley L. K., Broos P. S., Garmire G. P., Bouwman J., Povich M. S., Feigelson E. D., Getman K. V., Kuhn M. A., 2014, ApJS, 213, 1
Werner M. W. et al., 2004, ApJS, 154, 1

Whitney B. A., Wood K., Bjorkman J. E., Wolff M. J., 2003, ApJ, 591, 1049
Williams J. P., Cieza L. A., 2011, ARA&A, 49, 67
Xu Y., Reid M. J., Zheng X. W., Menten K. M., 2006, Science, 311, 54
Yasui C., Kobayashi N., Tokunaga A. T., Saito M., 2014, MNRAS, 442, 2543
Zavagno A., Pomarès M., Deharveng L., Hosokawa T., Russeil D., Caplan J., 2007, A&A, 472, 835

SUPPORTING INFORMATION

Supplementary data are available at *MNRAS* online.

Table 3. YSOs from 2MASS, IRAC/MIPS and X-ray data for the cluster area.

Table 4. Magnitudes, age and mass of the YSOs in the cluster region.

Please note: Oxford University Press is not responsible for the content or functionality of any supporting materials supplied by the authors. Any queries (other than missing material) should be directed to the corresponding author for the article.

This paper has been typeset from a TEX/LATEX file prepared by the author.